Citation for the original published paper:
S. Roger, C. Botella-Mascarell, D. Lloria, M. Cobos and G. Fodor, "Low-complexity AoA and AoD Estimation in the Transformed Spatial Domain for Millimeter Wave MIMO Channels," 2021 IEEE 32nd Annual International Symposium on Personal, Indoor and Mobile Radio Communications (PIMRC), 2021, pp. 1-6, doi: 10.1109/PIMRC50174.2021.9569292.

Low-complexity AoA and AoD Estimation in the Transformed Spatial Domain for Millimeter Wave MIMO Channels

Sandra Roger, Carmen Botella-Mascarell, Diego Lloria, Maximo Cobos
Computer Science Department
Universitat de València
46100 Burjassot (Valencia), Spain
sandra.roger@uv.es

Gábor Fodor
Ericsson Research
KTH Royal Institute of Technology
16400 Stockholm, Sweden
gaborf@kth.se

***Abstract*—High-accuracy angle of arrival (AoA) and angle of departure (AoD) estimation is critical for cell search, stable communications and positioning in millimeter wave (mmWave) cellular systems. Moreover, the design of low-complexity AoA/AoD estimation algorithms is also of major importance in the deployment of practical systems to enable a fast and resource-efficient computation of beamforming weights. Parametric mmWave channel estimation allows to describe the channel matrix as a combination of direction-dependent signal paths, exploiting the sparse characteristics of mmWave channels. In this context, a fast Transformed Spatial Domain Channel Estimation (TSDCE) algorithm was recently proposed to perform parametric channel estimation with low complexity, which in turn results in a full characterization of the transmitting and receiving angles for dominant signal paths. In this paper, we analyze the AoA/AoD estimation capability and accuracy of the TSDCE algorithm in detail. We find that the TSDCE algorithm has a significant performance advantage with respect to the traditional approach, which is based on frequency domain processing, in complexity-constrained environments, especially at high signal-to-noise ratios.**

***Index Terms*—mmWave, channel estimation, MIMO, analog beamforming, transformed spatial domain**

I. Introduction

Millimeter wave (mmWave) communications are one of the main technology drivers towards achieving high data rates in 5G and beyond 5G (B5G) systems. Their use was motivated by the scarcity of radio spectrum in conventional cellular bands [1], [2]. Communication in high frequency bands, however, poses a major challenge due to high propagation losses. To compensate for such propagation losses, mmWave systems implement beamforming techniques with highly directional beams that increase the gain of the link between transmitter (Tx) and receiver (Rx). This gain is achieved in practice by using antenna arrays with a high number of elements (in the order of several tens or hundreds), taking advantage of the small physical size of the antenna elements at these frequencies, which makes their implementation feasible.

B5G networks, such as 6G, will continue exploring the use of mmWave frequencies, extending the spectrum usage to the Terahertz (Hz) frequency range. Improved channel models, including aspects such as spatial and frequency consistency, are required to properly model communication in these bands [3]. In fact, advanced and fast channel estimation is a cornerstone step in any localization and sensing method. B5G/6G enablers, such as beamspace processing for accurate positioning, highly rely on obtaining profiles of channel angles and delays. Actually, estimation of the angle of arrival (AoA) and angle of departure (AoD) are fundamental to dynamically manage the beams, specially in non line-of-sight conditions. An example of advanced AoA and AoD tracking can be found in, for instance, [4].

This paper focuses on assessing the AoA and AoD estimation capability of a method previously proposed to estimate parametric mmWave multiple input multiple output (MIMO) channels in the transformed spatial domain, referred to as Transformed Spatial Domain Channel Estimation (TSDCE) [5]. The TSDCE method relies on a specific discrete Fourier transform (DFT)-based codebook of analog beamforming vectors, ordered in a way such that the observation matrix corresponds to the two-dimensional DFT (2D-DFT) of a sum of complex sinusoids in additive white Gaussian noise (AWGN). Since each sinusoid characterizes an angular component of the multipath channel between the Tx and Rx nodes in what is called the transformed spatial domain, the AoA and AoD of the multiple paths can be estimated from their associated sinusoids in the mixture. In [5], we evaluated the joint performance of the AoAs, AoDs and the path complex coefficients estimation, using the normalized mean square error (NMSE) of the estimated channel matrix as performance metric. The results showed that the TSDCE outperformed several state-of-the-art benchmarks at high signal-to-noise ratio (SNR). Among the selected benchmarks, the most competitive one in terms of performance is the DFT-based Channel Estimation Algorithm (DFT-CEA) proposed in [6]. DFT-CEA estimates the channel

Sandra Roger would like to thank the Spanish Ministry of Science, Innovation and Universities (RYC-2017-22101 Grant), and the Generalitat Valenciana (GVA) (GV/2020/046 Project). This work was also supported by the Spanish State Research Agency (PID2020-113785RB-100/AEI 10.13039/501100011033), and the GVA (AICO/2020/154 Project).

in the frequency domain after applying a 2D-DFT to an initial channel estimate. This benchmark is also considered in this work for comparison.

The remainder of the paper is structured as follows. Section II describes the system model. In Section III, the selected codebook for training is described and the TSDCE method is introduced. Section IV evaluates the AoA/AoD estimation performance and complexity of the TSDCE through numerical simulations, including a comparison with the DFT-CEA scheme for benchmarking. Finally, Section V draws the main conclusions of this work.

Notations: Bold uppercase $\mathbf{A}$ denotes a matrix and bold lowercase $\mathbf{a}$ denotes a column vector. Superscripts *, ^{T}, ^{H} and $^{-1}$ denote conjugate, transpose, conjugate transpose and inverse of a matrix, respectively. $[\mathbf{A}]_{q,p}$ is the (q,p)-th entry of $\mathbf{A}$, and $\|\mathbf{A}\|_F$ is the Frobenius norm. $\mathcal{CN}(m,\sigma^2)$ is a complex Gaussian random variable with mean m and variance σ^2. The magnitude and phase of a complex number are denoted by $|\cdot|$ and $\angle(\cdot)$, respectively. Finally, $\mathbb{C}$ and $\mathbb{R}^+$ denote the set of complex and positive real numbers, respectively.

II. System Model

A. Millimeter Wave Channel and Signal Model

The system model, depicted in Fig. 1, comprises a single-user mmWave geometric channel, where both the Tx and Rx are equipped with a uniform linear array of n_t and n_r antenna elements, respectively. L denotes the number of scatterers, each of which contributes with a single Tx-Rx propagation path, as in [7]–[9]. The complex channel coefficient of the l-th path is defined by α_l, $l = 1,\dots,L$, while ψ_l and ϕ_l stand for the AoA and AoD of the l-th path, respectively. The full parametric channel model is then conveniently characterized as:

$$\mathbf{H}(\boldsymbol{\theta}) = \sqrt{n_t n_r}\sum_{l=1}^{L}\alpha_l \mathbf{a}_r(\psi_l)\mathbf{a}_t^H(\phi_l), \tag{1}$$

where $\boldsymbol{\theta} \triangleq [|\alpha_1|,\angle\alpha_1,\phi_1,\psi_1,\dots,|\alpha_L|,\angle\alpha_L,\phi_L,\psi_L]^T$ is the parameter vector.

This channel model assumes that the α_l-s are independent identically distributed (i.i.d.) random variables with distribution $\alpha_l \sim \mathcal{CN}(0,\sigma_\alpha^2/L)$, while the AoAs ($\psi_l$) and AoDs ($\phi_l$) are drawn from a uniform distribution $\in [0,2\pi]$. The antenna array responses at the Tx and Rx, assuming half-wavelength antenna separation, can be expressed as

$$\mathbf{a}_t(\phi_l) = \frac{1}{\sqrt{n_t}}[1,\, e^{-j\pi\cos\phi_l},\cdots,e^{-j\pi(n_t-1)\cos\phi_l}]^T, \tag{2}$$

$$\mathbf{a}_r(\psi_l) = \frac{1}{\sqrt{n_r}}[1, e^{-j\pi\cos\psi_l},\cdots,e^{-j\pi(n_r-1)\cos\psi_l}]^T. \tag{3}$$

The value of the parameter L, although unknown a priori, has been proved by measurements at mmWave frequencies to be low due to the sparseness of the channel [10]. For the sake of simplicity, the dependence of Eq. (1) on the parameter vector $\boldsymbol{\theta}$ is omitted in the following.

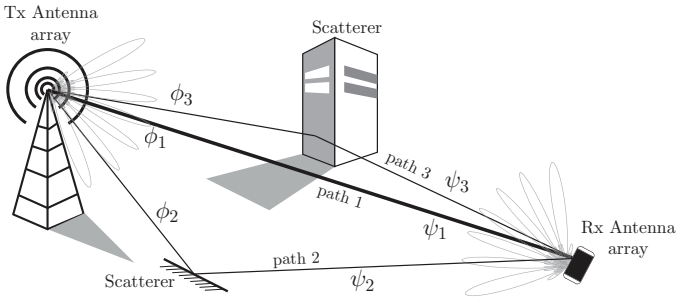

Fig. 1: Spatial channel model.

B. Pilot-based open-loop channel estimation

A mmWave system using analog beamforming (ABF) is considered, with Tx and Rx antennas connected to single Radio Frequency (RF) chains by means of a network of digitally controlled phase-shifters. Following previous works such as [8], the beam search space is given by a codebook comprising P and Q codewords or directions at the Tx and Rx side, respectively, which translate into quantized angles $\bar{\phi}_p$, $p = 0,1,\dots,P-1$ and $\bar{\psi}_q$, $q = 0,1,\dots,Q-1$. For subsequent channel estimations, a pilot-based training phase is carried out. In this case, a pilot symbol is transmitted, and received, through all possible directions. Assuming that $\mathbf{f}_p \in \mathbb{C}^{n_t\times 1}$ and $\mathbf{w}_q \in \mathbb{C}^{n_r\times 1}$ stand for the RF beamforming vectors at the Tx and Rx, respectively, the signal for the (q,p)-th pair of directions is given by

$$y_{q,p} = \sqrt{\rho}\,\mathbf{w}_q^H\mathbf{H}\mathbf{f}_p\,\mathrm{s} + \mathbf{w}_q^H\mathbf{n}, \tag{4}$$

where $\rho \in \mathbb{R}^+$ is the transmit power. The noise term $\mathbf{n} \sim \mathcal{CN}(0,\boldsymbol{\Sigma}_\mathbf{n})$ is a complex AWGN $1\times n_r$ vector with covariance $\boldsymbol{\Sigma}_\mathbf{n} = \sigma_n^2\mathbf{I}_{n_r}$, where $\mathbf{I}_{n_r}$ denotes the $n_r \times n_r$ identity matrix. Then, the system SNR is given by ρ/σ_n^2. For the sake of simplicity, the symbol s is set to 1 in what follows.

The observation matrix is obtained after transmitting the pilot symbol through the $Q \times P$ direction combinations

$$\mathbf{Y} = \sqrt{\rho}\,\mathbf{W}^H\mathbf{H}\mathbf{F} + \mathbf{N} = \sqrt{\rho}\,\mathbf{G}(\boldsymbol{\theta}) + \mathbf{N}, \tag{5}$$

where $\mathbf{W} = [\mathbf{w}_0,\dots,\mathbf{w}_{Q-1}] \in \mathbb{C}^{n_r\times Q}$ and $\mathbf{F} = [\mathbf{f}_0,\dots,\mathbf{f}_{P-1}] \in \mathbb{C}^{n_t\times P}$. The noise matrix $\mathbf{N} \in \mathbb{C}^{Q\times P}$ contains i.i.d. $\sim \mathcal{CN}(0,\sigma_n^2)$ elements, and $\mathbf{G} \in \mathbb{C}^{Q\times P}$ encodes the channel information $\boldsymbol{\theta}$. The effect of the different scatterers can be separated to write the observation matrix as a sum of path contributions $\mathbf{G}^{(l)}(\boldsymbol{\theta}_l) \in \mathbb{C}^{Q\times P}$, each one being dependent on a parameter vector $\boldsymbol{\theta}_l = [|\alpha_l|,\angle\alpha_l,\phi_l,\psi_l]^T$ as

$$\mathbf{Y} = \sqrt{\rho}\sum_{l=1}^{L}\mathbf{G}^{(l)}(\boldsymbol{\theta}_l) + \mathbf{N}. \tag{6}$$

Assuming that the beamforming/combining vectors are designed to match the array response [8], i.e. $\mathbf{f}_p = \mathbf{a}_t(\bar{\phi}_p)$

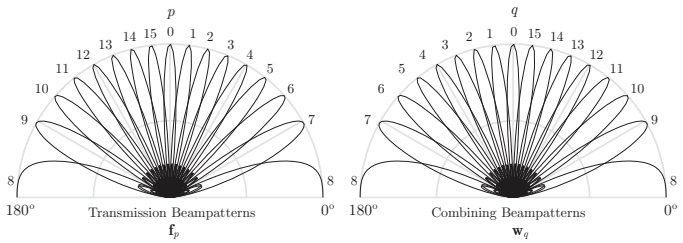

Fig. 2: Beampatterns for $n_T = n_R = 16$ and $Q = P = 16$.

and $\mathbf{w}_q = \mathbf{a}_r(\bar{\psi}_q)$, the elements $g_{q,p}^{(l)} = \left[\mathbf{G}^{(l)}(\boldsymbol{\theta}_l)\right]_{q,p}$ are given by

$$g_{q,p}^{(l)}(\boldsymbol{\theta}_l) = A_l \frac{1 - e^{-j\pi n_r(\cos\psi_l - \cos\bar{\psi}_q)}}{1 - e^{-j\pi(\cos\psi_l - \cos\bar{\psi}_q)}} \frac{1 - e^{j\pi n_t(\cos\phi_l - \cos\bar{\phi}_p)}}{1 - e^{j\pi(\cos\phi_l - \cos\bar{\phi}_p)}}, \tag{7}$$

where $A_l = \alpha_l/\sqrt{n_t n_r}$. Note that the observation matrix is sensitive to $\cos\phi_l$ and $\cos\psi_l$, whereas the actual AoDs and AoAs cover the range $[0, 2\pi]$. Hence, the quantized angles $\bar{\phi}_p$ and $\bar{\psi}_q$ only need to consider the range $[0, \pi]$.

III. Transformed Spatial Domain Channel Estimation

A. DFT-based Codebook

The TSDCE method considered in this work relies on the fact that, under a proper design of a DFT-based codebook for ABF, the observation matrix $\mathbf{Y}$ corresponds to the 2D-DFT of a sum of windowed complex sinusoids embedded in AWGN. This motivates solving the channel estimation problem in the transformed spatial domain, where the AoA and AoD for each channel path can be estimated by retrieving their associated angular frequencies:

$$\omega_{\psi_l} = -\pi\cos(\psi_l), \quad \omega_{\phi_l} = \pi\cos(\phi_l). \tag{8}$$

As shown in [5], each Eq. (7) corresponds to the 2D-DFT with $Q \times P$ bins of a windowed complex sinusoid provided that

$$e^{-j\pi\cos(\bar{\psi}_q)} = e^{j\frac{2\pi}{Q}q}, \quad q = 0, 1, \ldots, Q-1, \tag{9}$$

$$e^{j\pi\cos(\bar{\phi}_p)} = e^{j\frac{2\pi}{P}p}, \quad p = 0, 1, \ldots, P-1. \tag{10}$$

The variables $\omega_{\psi_l}, \omega_{\phi_l} \in [-\pi, \pi]$ denote the angular frequencies of such complex sinusoid in each spatial direction, where the vertical direction is related to the AoA and the horizontal direction is related to the AoD. It follows that parameter vector for the l-th path in the transformed spatial domain becomes $\boldsymbol{\omega}_l = [|\alpha_l|, \angle\alpha_l, \omega_{\phi_l}, \omega_{\psi_l}]^T$.

To satisfy Eqs. (9) and (10), the following conditions are set on the selected codebook angles

$$\cos(\bar{\phi}_p) = \mathcal{W}_{[-1,1]}\left(\frac{2p}{P}\right), \quad \cos(\bar{\psi}_q) = \mathcal{W}_{[-1,1]}\left(-\frac{2q}{Q}\right), \tag{11}$$

where $\mathcal{W}_{[a,b]}(x) \triangleq x - (b-a)\left\lceil \frac{x-b}{b-a} \right\rceil$ is the $[a, b]$ wrapping operator with $\lceil\cdot\rceil$ denoting the ceiling function. The above conditions imply simultaneously a uniform quantization in the range $[-1, 1]$ for the cosine of the codebook angles and a specific codebook ordering at the Tx and Rx. An example of the resulting beampatterns at the Tx and Rx for $Q = P = 16$ in a system with $n_T = n_R = 16$ antennas is shown in Fig. 2.

Taking into account Eqs. (2) and (3) together with the relationships of Eq. (8), the elements $h_{m,n} = [\mathbf{H}]_{m,n}$ can be written as

$$h_{m,n} = \sum_{l=1}^{L} \alpha_l e^{j\left(\omega_{\psi_l} m + \omega_{\phi_l} n\right)}, \tag{12}$$

indicating that the channel consists of a sum of L complex sinusoids. If the proposed DFT-based codebook is selected as in Eq.(11), the 2D-IDFT of the observation matrix $\mathbf{Y}$, expressed as $\mathbf{D}$, results in the following elements $d_{m,n} = [\mathbf{D}]_{m,n}$ in the transformed spatial domain

$$d_{m,n}(\boldsymbol{\omega}) = \begin{cases} \sum_{l=1}^{L} A_l e^{j\left(\omega_{\psi_l} m + \omega_{\phi_l} n\right)} + z_{m,n}, & \text{if } m < n_r,\ n < n_t \\ z_{m,n}, & \text{elsewhere} \end{cases}, \tag{13}$$

where $z_{m,n}$ belongs to a zero-mean complex Gaussian noise distribution with variance $\sigma_z^2 = \frac{1}{QP}\sigma_n^2$. The comparison of Eqs. (13) and (12), allows to identify that the $n_r \times n_t$ upper-left submatrix of $\mathbf{D}$ is just a scaled and noisy version of $\mathbf{H}$, where its spatial frequencies on the vertical and horizontal axes contain the directional information of the different channel paths.

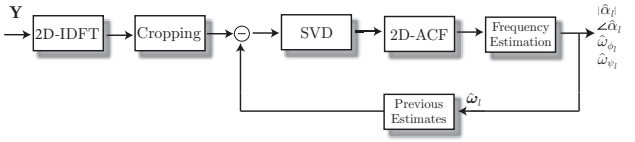

Fig. 3: Block diagram of the TSDCE algorithm.

B. TSCDE method

TSDCE is an iterative algorithm whose steps are summarized in Fig. 3. Starting from the most powerful path component ($l = 1$), the first step is based on performing the 2D-IDFT to the observation matrix $\mathbf{Y}$ to obtain $\mathbf{D}$. Next, a cropping step is performed to extract the upper-left submatrix containing the informative part of matrix $\mathbf{D}$, denoted as $\bar{\mathbf{D}}_{\mathbf{C}} \in \mathbb{C}^{n_r \times n_t}$. Then, an estimate of the contribution corresponding to the most powerful path component is obtained after performing the singular value decomposition (SVD) of $\bar{\mathbf{D}}_{\mathbf{C}}$ to achieve a rank-one approximation through the dominant singular-value, resulting in matrix $\widetilde{\mathbf{D}}_{\mathbf{C}}$.

The second step is based on the denoising properties of the unbiased 2D sample autocorrelation function (ACF), which is applied to $\widetilde{\mathbf{D}}_{\mathbf{C}}$ to obtain a new matrix $\mathbf{R} \in \mathbb{C}^{n_r \times n_t}$. The phase angle in elements of matrix $\mathbf{R}$ contain the necessary information for the estimation of ω_{ψ_l} and ω_{ϕ_l}. More specifically, the phases of the first row and the first column of $\mathbf{R}$ provide the required frequency information.

In a third step, spatial frequency estimation is performed. Following the discussion in [5], the frequency estimation

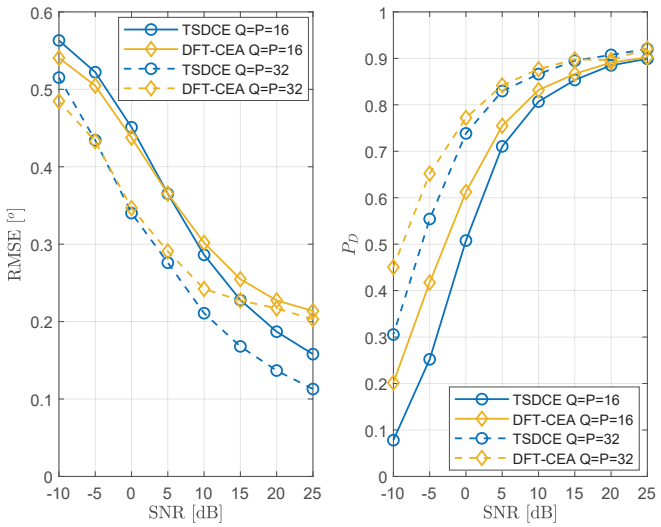

Fig. 4: Root Mean Square Error (RMSE) and P_D of angles estimated with TSDCE and DFT-CEA considering $L = 3$ and $n_t = n_r = 16$, and different values of SNR and codebook sizes.

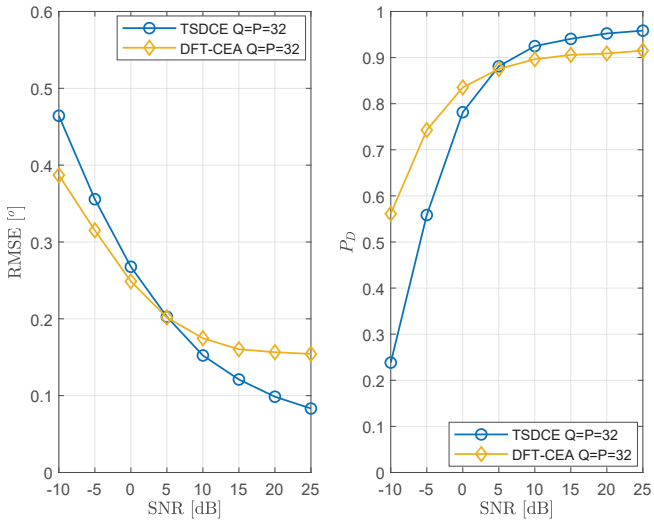

Fig. 5: RMSE and P_D of angles estimated with TSDCE and DFT-CEA for different values of SNR, considering $L = 3$ and $n_t = n_r = 32$.

can be obtained by estimating the slopes of the unwrapped phase sequences (derived in the second step) in both the vertical and horizontal directions. The solution involves a four-step process: unwrapping the phases, estimating the slope by weighted least squares (WLS), designing the weights for the WLS optimization problem and estimating the path complex coefficient (both $|\hat{\alpha}_1|$ and $\angle\hat{\alpha}_1$).

Estimating the rest of the paths of the channel follows the same steps as above, but the spatial domain observation matrix $\bar{\mathbf{D}}_{\mathbf{C}}$ is updated by means of a successive interference cancellation (SIC) approach, so that the contribution from already reconstructed path components is suppressed (see Eq. (76) in [5]).

The iteration criterion in the TSDCE algorithm can be limited to a given number of desired path components to be extracted, without preventing the use of more realistic criteria. Once the estimates of the L path components are available after the first execution of the algorithm, these can be effectively used to cancel all the disturbing path contributions from the original observation, leading to enhanced estimates for all paths. To this end, the method has a parameter called K which allows to perform more estimation runs to refine the solution. As shown in [5], the method exhibits a SNR gain when $QP > n_t n_r$.

IV. Performance Evaluation

In this section, the AoA/AoD estimation performance and complexity of the TSDCE are obtained through numerical simulations. For SNR values ranging from -10 dB to 25 dB, 10^5 random realizations are generated following the observation model given in Eq. (5) with $\rho = 1$, i.e. the SNR definition is $1/\sigma_n^2$. AoA and AoD angles are drawn from a uniform distribution in the range $[0, \pi]$, whereas channel coefficients are drawn from a zero mean complex Gaussian distribution with variance $1/L$. The K parameter in the TSDCE is set to 3 for a good complexity versus performance tradeoff [5].

As a benchmark for comparison, we consider the DFT-based scheme (DFT-CEA) proposed in [6]. This method operates in the frequency domain after applying a 2D-DFT of N_{DFT} points to an initial channel estimate, and it obtains the AoAs and AoDs from the DFT peaks through iterative cancellation. As in [6], we set $N_{DFT} = 1024$.

A. AoA and AoD performance

To assess the AoA/AoD estimation accuracy, the RMSE of the angle measurements, calculated as

$$\text{RMSE} = \sqrt{\frac{1}{|\mathcal{N}|}\sum_{i\in|\mathcal{N}|}(\vartheta_i - \hat{\vartheta}_i)^2}, \tag{14}$$

and the probability of detection (P_D) at different SNRs are obtained. A detection is considered successful if the associated RMSE $\leq 1°$. According to this definition, the set of successfully detected angles is denoted by $\mathcal{N}$, while ϑ_i considers any AoA or AoD.

Fig. 4 analyzes the AoA/AoD estimation capability of the TSDCE and DFT-CEA methods with $L = 3$ in terms of RMSE and P_D, considering $n_T = n_R = 16$ and codebooks with $Q = P = 16$ and $Q = P = 32$ elements. At low SNRs, the DFT-CEA outperforms the TSDCE, since it exhibits a higher P_D than the TSDCE with similar RMSE. At medium to high SNRs, the TSDCE shows superior performance, since both methods present similar P_D, having the TSDCE lower RMSE values. Regarding the codebook sizes, both methods provide enhanced angle estimations when $Q = P = 32$. The latter

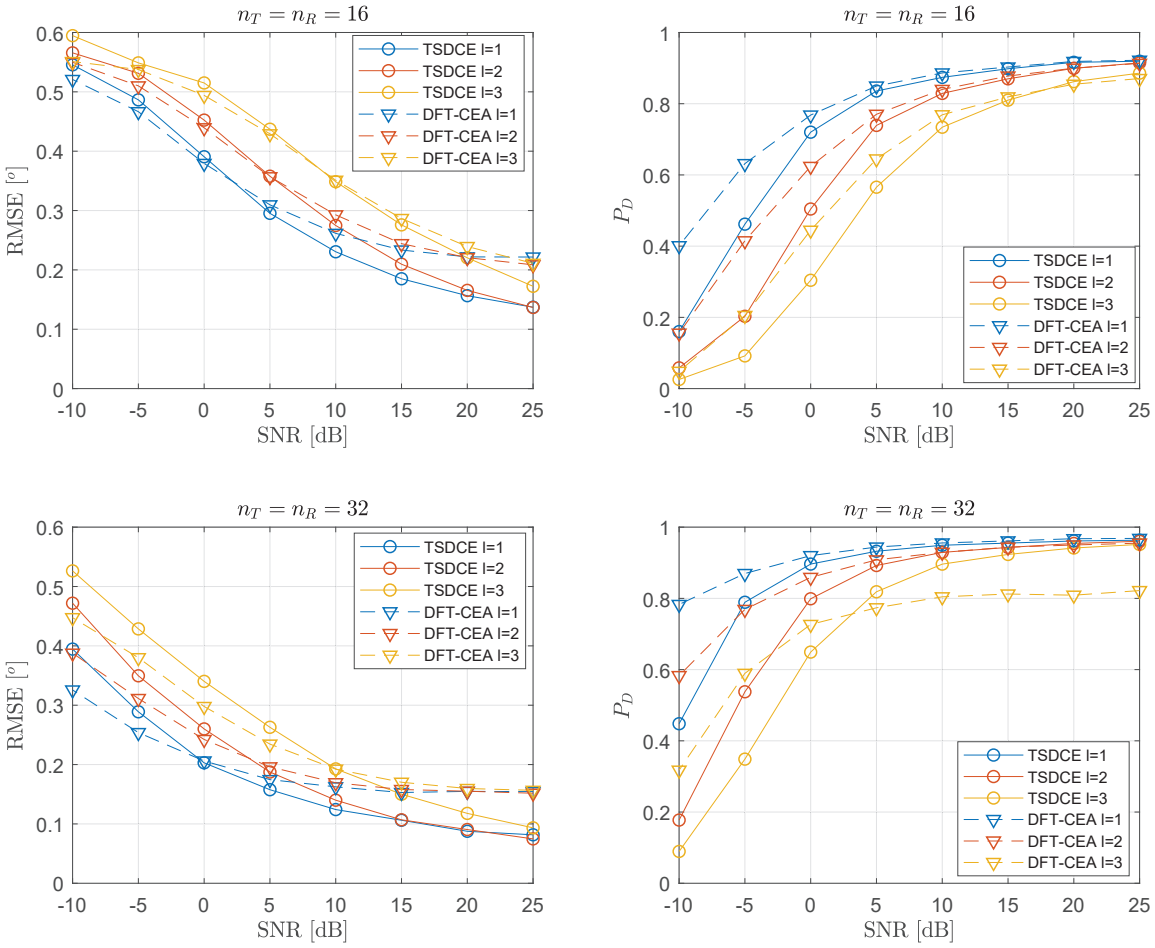

Fig. 6: RMSE and P_D of angles estimated with TSDCE and DFT-CEA for each channel path, considering $L = 3$ and different values of SNR and antennas.

result is consistent with the expected SNR gain provided by having more codebook elements than antennas [5].

In Fig. 5, the number of antennas is increased to $n_T = n_R = 32$, setting the codebook sizes to $Q = P = 32$. It can be observed that the performances of both methods in terms of RMSE and P_D are enhanced. In constrast to the results shown in Fig. 4, the TSDCE outperforms the DFT-CEA at medium to high SNRs not only regarding RMSE values but also in terms of P_D. For SNRs below 5 dB, the DFT-CEA is a more competitive approach, providing lower RMSE and significantly higher P_D than the TSDCE.

Fig. 6 shows the AoA/AoD estimation results independently for each path in a channel with $L = 3$. Top subplots consider $n_T = n_R = 16$ and $Q = P = 16$, whereas bottom subplots correspond to the $n_T = n_R = 32$ and $Q = P = 32$ case. From the $n_T = n_R = 16$ results, we can observe that the TSDCE and DFT-CEA achieve the same P_D at high SNR, having the TSDCE lower RMSE for all paths. Also at high SNR, the estimation performances for the first and second paths (see $l = 1$ and $l = 2$ curves) converge, while the angle RMSE of the third path ($l = 3$) is higher. This effect is observed for both estimation methods. When $n_T = n_R = 32$, the TSDCE starts to outperform the DFT-CEA from a lower SNR point. As in the previous antenna configuration, the performances for the first and second paths converge, while the third path estimate is poorer. This effect is specially striking when looking at the DFT-CEA, $l = 3$, P_D curve, where it can be seen that the P_D for the third path is substantially worse than for the rest.

B. *Computational complexity analysis*

The computational complexities of the TSDCE and DFT-CEA methods are compared in terms of average elapsed time to run the Matlab implementation of each algorithm. The simulations are carried out in a desktop computer with an Intel® Core™ i7-8700 Central Processing Unit at 3.20 GHz.

Fig. 7 compares the average runtime in seconds needed to estimate the AoA and AoD with the two considered methods, when the number of antennas is increased. To narrow down the possible options, two values for the number of estimated channel paths are selected ($L = 3$ and $L = 4$) and three values for the number of antennas ($n_T = \{16, 32, 64\}$). In all cases, we set $n_t = n_r = Q = P$. It can be first noticed that

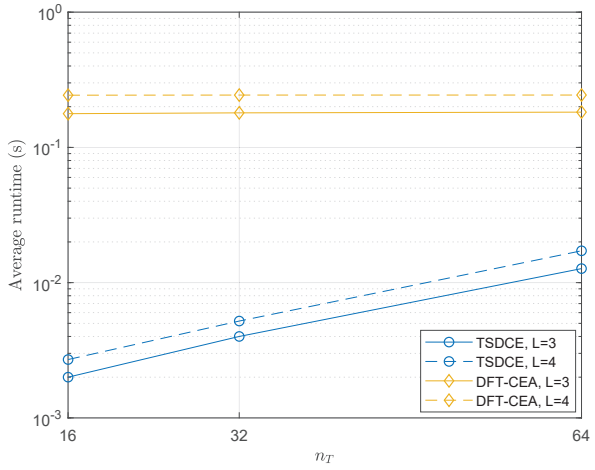

Fig. 7: Average runtime of TSDCE and DFT-CEA for different numbers of transmit antennas and channel paths, considering $n_t = n_r = Q = P$.

the runtime of the DFT-CEA is constant with the number of antennas. This result is reasonable, since the dominant term of its computational complexity is the DFT operation, whose size is kept to $N_{DFT} = 1024$ in all the configurations. Regarding the TSDCE, its runtime increases with the number of antennas, but its values remain in all evaluated cases between one and two orders of magnitude below those of the DFT-CEA. When the number of channel paths is increased from $L = 3$ to $L = 4$, the runtime of both methods increases similarly. This result is also consistent, since both methods follow an iterative cancellation approach to estimate channel paths, and the runtime increase is caused by the estimation of the fourth path.

Finally, we evaluated the impact of the codebook size on the average runtime for both methods. To this end, we set $n_T = n_R = 16$ and compared the runtimes with $Q = P = 16$ and $Q = P = 32$. The TSDCE runtime increases from 2ms to 2.8ms for $L = 3$ and from 2.7ms to 3.5ms for $L = 4$, i.e., it involves an absolute runtime increase of 0.8ms. On the other hand, the DFT-CEA runtime does not vary with the codebook size due to the effect of the dominant DFT term.

V. Conclusion

In this paper, the performance and complexity of AoA/AoD estimation in the transformed spatial domain have been evaluated in a mmWave MIMO channel. In particular, transformed spatial domain estimation (TSDCE) has been compared to an iterative channel estimation approach based on the Discrete Fourier Transform (DFT-CEA). When comparing the root mean square error of angles and probability of detection in a set of antenna and channel configurations, the TSDCE outperforms the DFT-CEA at medium to high signal-to-noise ratio (SNR) values. The use of training codebooks with more elements than the number of antennas enhances both methods. The performance advantage of TSDCE over DFT-CEA is more significant when considering 32 antennas instead of 16. It is also observed that, in a channel with three paths, the estimation performance of the first and second paths converge at high SNR. However, the probability of detection for the third path is substantially worse.

From the complexity analysis results, which evaluated average runtime, it is observed that the DFT-CEA runtime remains constant when the number of antennas and/or codebook elements increases. On the contrary, the TSDCE runtime increases with the number of antennas and/or codebook elements. Despite this, the TSDCE runtime remains one or two orders of magnitude below the DFT-CEA runtime in all cases, showing that it is a substantially faster solution to estimate the AoA and AoD. In fact, the TSDCE performance loss at low SNR could be worthwile for complexity-constrained applications. Finally, it was observed that estimating an additional path increases the runtime similarly for both methods.

References

[1] W. Roh, J. Seol, J. Park, B. Lee, J. Lee, Y. Kim, J. Cho, K. Cheun, and F. Aryanfar, "Millimeter-wave beamforming as an enabling technology for 5G cellular communications: theoretical feasibility and prototype results," *IEEE Communications Magazine*, vol. 52, no. 2, pp. 106–113, February 2014.

[2] J. G. Andrews, T. Bai, M. N. Kulkarni, A. Alkhateeb, A. K. Gupta, and R. W. Heath, "Modeling and analyzing millimeter wave cellular systems," *IEEE Transactions on Communications*, vol. 65, no. 1, pp. 403–430, Jan 2017.

[3] C. De Lima, D. Belot, R. Berkvens, A. Bourdoux, D. Dardari, M. Guillaud, M. Isomursu, E.-S. Lohan, Y. Miao, A. N. Barreto, M. R. K. Aziz, J. Saloranta, T. Sanguanpuak, H. Sarieddeen, G. Seco-Granados, J. Suutala, T. Svensson, M. Valkama, B. Van Liempd, and H. Wymeersch, "Convergent communication, sensing and localization in 6G systems: An overview of technologies, opportunities and challenges," *IEEE Access*, vol. 9, pp. 26 902–26 925, 2021.

[4] N. Garcia, H. Wymeersch, and D. T. M. Slock, "Optimal precoders for tracking the AoD and AoA of a mmwave path," *IEEE Transactions on Signal Processing*, vol. 66, no. 21, pp. 5718–5729, 2018.

[5] S. Roger, M. Cobos, C. Botella-Mascarell, and G. Fodor, "Fast channel estimation in the transformed spatial domain for analog millimeter wave systems," *IEEE Transactions on Wireless Communications*, vol. in press, 2021.

[6] S. Montagner, N. Benvenuto, and P. Baracca, "Channel Estimation Using a 2D DFT for Millimeter-Wave Systems," in *2015 IEEE 81st Vehicular Technology Conference (VTC Spring)*, 2015, pp. 1–5.

[7] O. E. Ayach, R. W. Heath, S. Abu-Surra, S. Rajagopal, and Z. Pi, "Low complexity precoding for large millimeter wave MIMO systems," in *2012 IEEE International Conference on Communications (ICC)*, 2012, pp. 3724–3729.

[8] C. Zhang, D. Guo, and P. Fan, "Tracking angles of departure and arrival in a mobile millimeter wave channel," in *2016 IEEE International Conference on Communications (ICC)*, May 2016, pp. 1–6.

[9] A. Alkhateeb, O. El Ayach, G. Leus, and R. W. Heath, "Channel estimation and hybrid precoding for millimeter wave cellular systems," *IEEE Journal of Selected Topics in Signal Processing*, vol. 8, no. 5, pp. 831–846, 2014.

[10] M. R. Akdeniz, Y. Liu, M. K. Samimi, S. Sun, S. Rangan, T. S. Rappaport, and E. Erkip, "Millimeter wave channel modeling and cellular capacity evaluation," *IEEE Journal on Selected Areas in Communications*, vol. 32, no. 6, pp. 1164–1179, 2014.